

# Delayed differential detection for absorption spectroscopy recovery

MENGLONG CONG<sup>\*</sup>, DANDAN SUN

Inner Mongolia University for the Nationalities, College of Physics and Electronic Information,  
No. 536, Huolinhe Street, Tongliao 028000, China

\*Corresponding author: congml@163.com

An elaborately designed system has been devoted to the recovery of the line shape function of absorption spectrum. Laser power passing through trace gas has been divided into the real-time and delayed components, and their difference, *i.e.* the equivalent of the first-order derivative spectrum, is recorded and integrated to reconstruct the absorption line profile. Since the real-time and delayed signals are derived from the only gas cell and photodetector, the elimination of background is more effective, relative to the general used double beam detection that involves two gas cells and photodetectors. Compared with the 1st harmonic detection used in the wavelength modulation spectroscopy, here the generation of derivative spectrum is achieved without modulating the injection current of laser. Additionally, the expensive lock-in amplifier working for wavelength modulation spectroscopy is replaced by a homemade device, which is made of an all-pass filter and an instrumentation amplifier. Therefore, the complexity and cost are significantly reduced, and the stability is improved. For the purpose of validation, recovering of the absorption spectroscopy is carried out using a methane sample at its  $R(3)$  absorption line of the  $2v_3$  overtone, and the obtained data are found to be in a high agreement with theoretical deductions.

Keywords: wavelength modulation spectroscopy (WMS), absorption, derivative spectrum, harmonic detection, laser diode.

## 1. Introduction

As a well-established method for *in situ* measurements of combustion parameters in the industrial environment [1–3], tunable diode laser absorption spectroscopy (TDLAS) [4, 5] accompanied by standard telecommunication used distributed feedback (DFB) diode laser provides significant advantages in selectivity and sensitivity. From the absorption spectrum, gas properties such as temperature, pressure, velocity and concentration can be exactly determined [6]. The compact structure and easily tuned wavelength have made DFB diode laser a suitable light source for a portable spectrometer, working generally in the near infrared (NIR) region [7]. Although direct detection gives a straightforward way to the absorption spectrum through the comparison between transmitted and referenced signals, the limit of detection (LOD) is poor because

of the extremely weak strength of absorption line, which belongs to the overtone or combination vibrational transitions around the NIR region [8]. Conversely, in the mid infrared region live abundant spectrum lines attached to the fundamental vibrational bands, with strong absorption intensity [9]. However, an unavoidable problem is the expensive laser source and photodetector. With the aid of frequency modulation spectroscopy (FMS), wavelength modulation spectroscopy (WMS), or many other techniques, the LOD of the system utilizing a single mode NIR diode laser for trace gas detection, has been successfully prompted to the order of ppmv [10].

Putting aside the common fundamentality that FMS and WMS both depend upon, the latter can be easily distinguished from the former, owing to the significant differences in terms of modulation parameters and detection technique. In WMS, the injection current of laser is usually ramped at a moderate frequency for scanning across the entire wavelength range of the selected absorption line. Meanwhile, a sinusoidal modulation with a frequency significantly higher than the scan frequency but much lower than the absorption half-width, is superimposed upon the swept signal for producing a modulated laser wavelength [11]. In contrast, as an offshoot of WMS, FMS is confined to the category where the frequency of modulation extends far beyond the half-width of absorption frequency [12].

Due to the interaction of modulated laser wavelength with the absorption feature, harmonics of the absorption spectrum are generated and can be collected using certain technique, such as phase sensitive detection [13]. Resulting from the collection of harmonic, the working frequency is elevated, which thus leads to the weakening of both the flicker and the laser noise [14]. In the condition of small modulation depth, the intensity of  $n$ -th harmonic will be proportional to the  $n$ -order derivative of the shape function of absorption feature [15]. Usually, the 1st harmonic (WMS-1f) is attractive to study for absorption spectrum since it could be directly recovered from the integration of first-order derivative spectrum. But unfortunately, in the case of injection-current tuned diode laser, the wavelength modulation is followed inevitably by laser intensity modulation (IM) [16], and the recovery of absorption spectrum is likely to be influenced by the RAM [17], which is a product of IM. Even though the RAM appearing in the 2nd harmonic is negligible for conventional telecommunication used DFB lasers, the spreading of WMS to high pressure or large-modulation-depth situations is still impeded by the need of the 1st harmonic normalization [18], as well as the distortion of signal due to cross-coupling between the predominantly linear IM and Fourier components of an absorption line [19].

In the work reported here, a novel strategy which is back-ground free and cost-effective is put forward to reconstruct the absorption line shape function. The experimental apparatus is sketched in Section 2. A homemade electronic device consists of an all-pass filter and an instrumentation amplifier is developed to produce the equivalent of first -order derivative spectrum. In Section 3, the operational regime of this apparatus is briefed. Several key issues, for instance, the means coping with the fluctuation of optic intensity caused by the sloping injection current of laser, and the appropriate time delay

for reconstructing the absorption spectrum, are discussed in detail. Finally, experiments using the mixture of  $\text{CH}_4$  and  $\text{N}_2$  are carried out and the results are shown in Section 4 for theory validation. To evaluate the stability and sensitivity, spectral absorbance derived from the integration of first-order derivative spectrum is compared with the software simulation using the Voigt line model and the optical parameters from HITRAN04 database [20].

## 2. Experimental setup

Figure 1 illustrates the scheme of our experimental apparatus. Two cylinders filled with high-purity  $\text{N}_2$  and  $\text{CH}_4$  are connected to a bank of mass flow controllers (Teledyne Hastings, HFC-302 with THPS-400 controller) for blending the gas components to the desired ratio. Through a nylon resin tube, the gas mixture is delivered to a stainless cell with an effective optical path length of 15.4 cm. The total pressure is gauged by a capacitance manometer (Setra Systems, MODEL720), and kept at  $1.01 \times 10^5$  Pa through controlling the velocity of gas flow. At the intervals of measurements, the stainless cell is nitrogen-flushed and emptied by a turbo molecular pump to an ultimate pressure of less than 133.3 Pa. The temperature along the axis is monitored by three type-K thermocouples which are attached to the middle and both end faces of the stain-

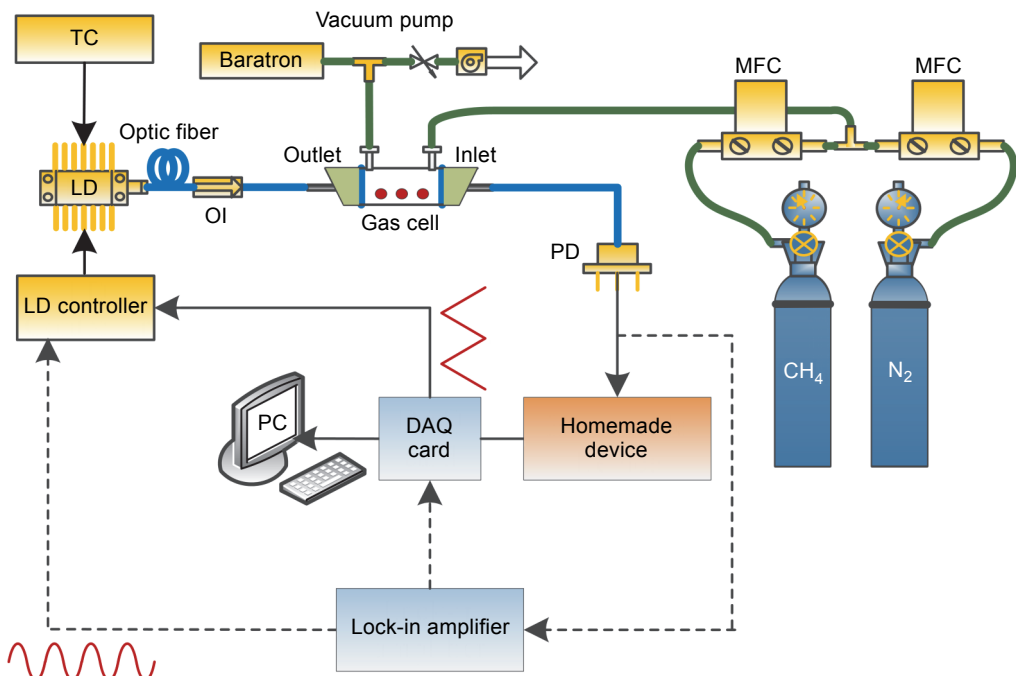


Fig. 1. Schematic diagram of the experimental setup; TC – temperature controller, MFC – mass flow controller, OI – optical isolator, PD – photodetector, and LD – laser diode.

less cell. A cylindrical ceramic fiber heater twining around the cell is PID controlled to maintain the inner temperature at about 296 K.

In a 14-pin commercial butterfly mount (Mitsubishi, FU-68PDF-V510), the thermistor and thermoelectric cooler are packaged along with the diode laser source for monitoring and regulating the temperature of laser. The coherent radiation of the laser source on a single mode is up to 10 mW, under the condition of 24 mA driving current and 305 K working temperature. The emitting wavelength is simultaneously manipulated by a low-noise laser current supply (Newport, Model 500B) and a high-precision laser temperature controller (ILX, Model LDT-5900C), to access the central value of 1.654  $\mu\text{m}$ , which matches the  $R(3)$  absorption transition of  $2\nu_3$  band for  $\text{CH}_4$ .

From a 16-bit data acquisition (DAQ) card, a 5 Hz saw-tooth waveform is sent to the input of the laser current controller for sweeping over the entire wavelength range of the target absorption transition. Before guided into the gas cell, the incident laser power is fiber coupled to an optical isolator to prevent the happening of system performance degradation induced by optical feedback scattering. After a single pass through the gas volume under test, the transmitted laser power is focused onto an InGaAs photodiode with  $1 \text{ mm}^2$  active area.

Both the phase-sensitive detection and the delayed differential detection can be implemented using the similar experimental system. For phase-sensitive detection, the lock-in amplifier (Signal Recovery Inc., Model 7265) is introduced to make a sinusoidal modulation on the lasing wavelength, and then it locks in the 1st harmonic of absorption spectroscopy. For delayed differential detection, the lock-in amplifier is replaced by a homemade electronic device for generating the 1st derivative spectrum, and the sinusoidal modulation of lasing wavelength is avoided.

The design of this homemade device is briefed in Fig. 2. In the device, the input is electronically divided. One of them, named as the delayed arm, is phase shifted by

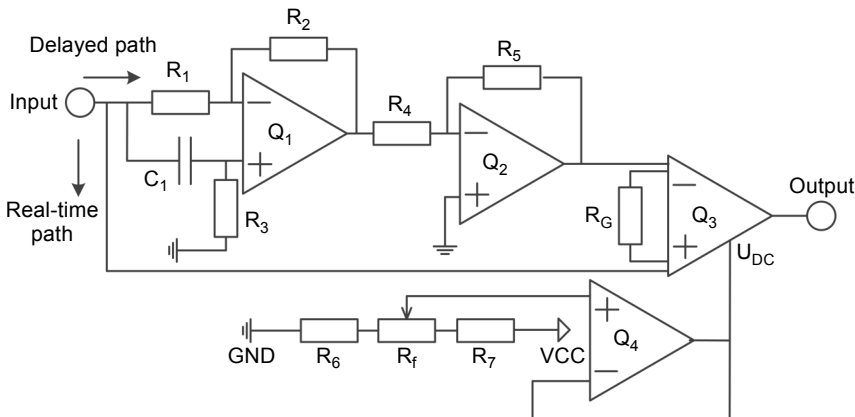


Fig. 2. Functional block diagram of the homemade electronic device. The following components were used in the device:  $Q_1$  and  $Q_2$  – OP470 low-noise op-amp,  $Q_3$  – AD8422 instrumentation amplifier, and  $Q_4$  – OP1177 low-noise op-amp.

an all-pass filter and deducted from the other one, which is called the real-time arm. Initial phase of the delayed arm is determined by resistor  $R_3$  and capacitor  $C_1$  that are mounted closely to  $Q_1$ . The inverted polarity is solved by a reverse phase amplifying circuit that consists of  $Q_2$ ,  $R_4$  and  $R_5$ . Difference of the delayed and real-time arms is amplified via an instrumentation amplifier  $Q_3$ , with its DC bias and gain set by resistors  $R_f$  and  $R_G$ , respectively. The analog output is digitized using the DAQ card, and captured into a PC programmed with LabVIEW for further data analysis.

### 3. Basic theory of derivative spectroscopy

The total injection current of DFB-LD, with the DC bias ( $i_{DC}$ ) and saw-tooth ( $i_{saw}(t)$ ) current components taken into account, is written as

$$i_{LD}(t) = i_{DC} + i_{saw}(t) = i_{DC} + k \left( \frac{t}{T_0} - \left\lfloor \frac{t}{T_0} \right\rfloor \right) \quad (1)$$

with  $\lfloor \cdot \rfloor$  being the round down function,  $k$  – the slope of saw-tooth current and  $T_0$  – the period.

From the total injection current of DFB-LD, the instantaneous optical wavelength output  $v_{opt}(t)$  and the optical power output  $P_{opt}(t)$  can be inferred

$$v_{opt}(t) = v_0 + \mu_{slope} i_{LD}(t) \quad (2)$$

$$P_{opt}(t) = P_0 + \eta_{slope} i_{LD}(t) \quad (3)$$

with  $v_0$  and  $P_0$  being the wave number and optical power respective to  $i_{DC}$ ,  $\mu_{slope}$  represents the current–wave number coefficient, and  $\eta_{slope}$  represents the current–power coefficient of the DFB-LD. For optical thin conditions ( $\alpha(v_{opt}) \ll 0.1$ ), the optical power  $P_{gas}(t)$  through gas absorption can be approximated to

$$\begin{aligned} P_{gas}(t) &= P_{opt}(t) \left\{ 1 - \alpha \left[ v_{opt}(t) \right] \right\} \\ &= \left\{ P_0 + \eta_{slope} \left[ i_{DC} + k \left( \frac{t}{T_0} - \left\lfloor \frac{t}{T_0} \right\rfloor \right) \right] \right\} \left\{ 1 - \alpha \left[ v_{opt}(t) \right] \right\} \end{aligned} \quad (4)$$

In Eq. (4),  $\alpha(v_{opt})$  is the spectral absorbance at the wavelength  $v_{opt}(t)$ , and can be expressed as a product of total pressure  $P$ , line strength  $S(T)$  at temperature  $T$ , absorption shape function  $g(v_{opt})$ , species mole fraction  $\chi$  and effective absorption length  $L$ :

$$\alpha \left[ v_{opt}(t) \right] = PS(T) g \left[ v_{opt}(t) \right] \chi L \quad (5)$$

After a single pass through the gas cell, the transmitted optical power  $P_{gas}(t)$  is delivered to a photodiode with the responsivity  $R$ . The photocurrent produced from the

photodiode is converted to voltage via a transconductance amplifier with the gain factor  $Z_{\text{TIA}}$ . The output of the transconductance amplifier is divided into two paths, with one of them delayed at time constant  $\tau$ :

$$U_{\text{RT}}(t) = Z_{\text{TIA}} R P_{\text{gas}}(t) \quad (6)$$

$$U_{\text{delay}}(t) = Z_{\text{TIA}} R P_{\text{gas}}(t - \tau) \quad (7)$$

The real-time signal  $U_{\text{RT}}(t)$  and the delayed signal  $U_{\text{delay}}(t)$  are fed to the inputs of an instrumentation amplifier with  $U_{\text{DC}}$  the tunable offset voltage, and their difference is amplified with a gain of  $G$

$$\begin{aligned} U_{\text{diff}}(t) &= G \left[ U_{\text{RT}}(t) - U_{\text{delay}}(t) \right] + U_{\text{DC}} \\ &= GZ_{\text{TIA}} R \left[ P_{\text{opt}}(t) - P_{\text{opt}}(t - \tau) \right] \\ &\quad - GZ_{\text{TIA}} R \left[ P_{\text{opt}}(t) \alpha[v_{\text{opt}}(t)] - P_{\text{opt}}(t - \tau) \alpha[v_{\text{opt}}(t - \tau)] \right] + U_{\text{DC}} \end{aligned} \quad (8)$$

In order to illustrate the elimination of background intuitively, the real-time signal, delayed signal and their difference are simulated in the absence of gas absorption and shown in Fig. 3. These waveforms are separated into the “valid” and “invalid” regions. The trigger of data acquisition is controlled by a soft timer to reserve the samples in “valid” region but get rid of those belong to “invalid” region.

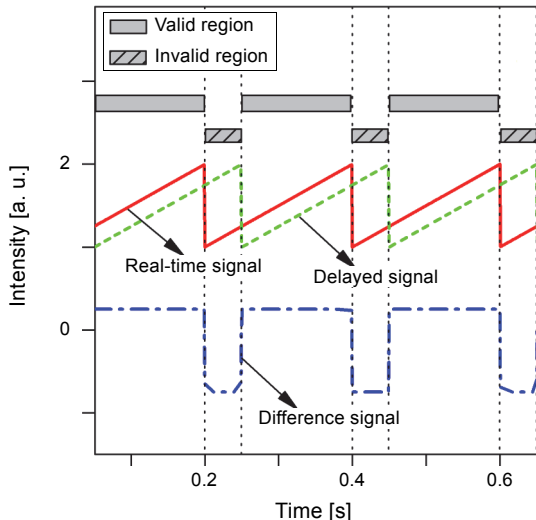


Fig. 3. The real-time signal (solid line), delayed signal (dashed line) and their difference (dash-dot line) in the absence of gas absorption.

From a fine tuning of the offset of instrumentation amplifier, the constant difference shown in the “valid” region can be minimized, and then Eq. (8) is simplified to

$$\begin{aligned} U_{\text{diff}}(\nu_{\text{opt}}) &= GZ_{\text{TIA}} R \left\{ P_{\text{opt}}(\nu_{\text{opt}}) \left[ \alpha(\nu_{\text{opt}} + \Delta\nu_m) - \alpha(\nu_{\text{opt}}) \right] \right. \\ &\quad \left. - \left[ P_{\text{opt}}(\nu_{\text{opt}}) - P_{\text{opt}}(\nu_{\text{opt}} + \Delta\nu_m) \right] \alpha(\nu_{\text{opt}} + \Delta\nu_m) \right\} \\ &\approx GZ_{\text{TIA}} R P_{\text{opt}}(\nu_{\text{opt}}) \left[ \alpha(\nu_{\text{opt}} + \Delta\nu_m) - \alpha(\nu_{\text{opt}}) \right] \end{aligned} \quad (9)$$

with the time index  $t$  converted to wave number  $\nu_{\text{opt}}$ , according to Eq. (2). When the wave number scanning is confined in a linear range, *e.g.*  $\Delta\nu_{\text{scan}}$ , the increment of wave number  $\Delta\nu_m$  can be determined directly by

$$\Delta\nu_m = \frac{\Delta\nu_{\text{scan}}}{T_0} \tau \quad (10)$$

Theoretically any value of the wave number increment can be realized, by directly adjusting the delay time  $\tau$ . But, indeed, it is not advisable to select a huge delay time, in that the approximation using in Eq. (9) will lead to a significant error. Likewise, the achievement of a tiny delay time is not recommended because this will lead to the drastic attenuation at the output of instrumentation amplifier, thereby reducing the signal-to-noise ratio (SNR).

After the normalization of  $U_{\text{diff}}(\nu_{\text{opt}})$  by the power spectrum of laser sweep, *i.e.* expression  $GZ_{\text{TIA}} R P(\nu_{\text{opt}})$ , the first-order derivatives of the spectral absorbance are

$$\alpha'(\nu_{\text{opt}}) = \frac{\alpha(\nu_{\text{opt}} + \Delta\nu_m) - \alpha(\nu_{\text{opt}})}{\Delta\nu_m} \quad (11)$$

From the integration of the above derivative, the spectral absorbance could be recovered.

## 4. Results and discussions

STEWART *et al.* [21] have indicated that the 1st Fourier coefficient of absorption spectroscopy experiences a peak while the laser wavelength  $\nu_L$ , the half-width at half-maximum (HWHM) of the selected gas absorption transition  $\Delta\nu_{\text{gas}}$ , and the absorption center  $\nu_0$  conform to

$$\nu_L = \frac{\Delta\nu_{\text{gas}}(\sqrt{3m^2 + 4} - 1)}{\sqrt{3} + \nu_0} \quad (12)$$

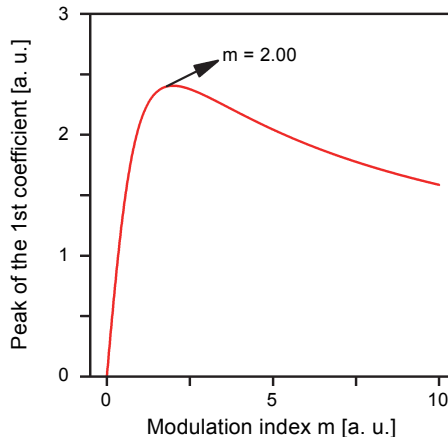


Fig. 4. Simulated peak of the 1st Fourier coefficient of absorption spectroscopy with the increase of modulation index  $m$ . The necessary spectral parameters are retrieved from HITRAN04 database.

According to Eq. (12), the dependence of the 1st Fourier coefficient of absorption spectroscopy on modulation index  $m$  ( $m = \Delta\nu_m/\Delta\nu_{\text{gas}}$ ) is simulated for 1% CH<sub>4</sub> diluted by N<sub>2</sub>, under  $1.01 \times 10^5$  Pa and 296 K. As could be seen from the result shown in Fig. 4, the peak occurs while  $m = 2.00$ . In the following experiments, the actually used  $m$  is initially set at 2.00 and then finely tuned for maximizing the amplitude of a signal.

For an impartial and objective comparison between delayed differential detection and phase-sensitive detection, experiments are implemented under identical conditions such as temperature, total pressure, gas samples, *etc.* Before the formal measurements using specimens, the laser emitting background is recorded to deal with the hardware-related parameters and transmission losses. Through normalizing the absorption-based

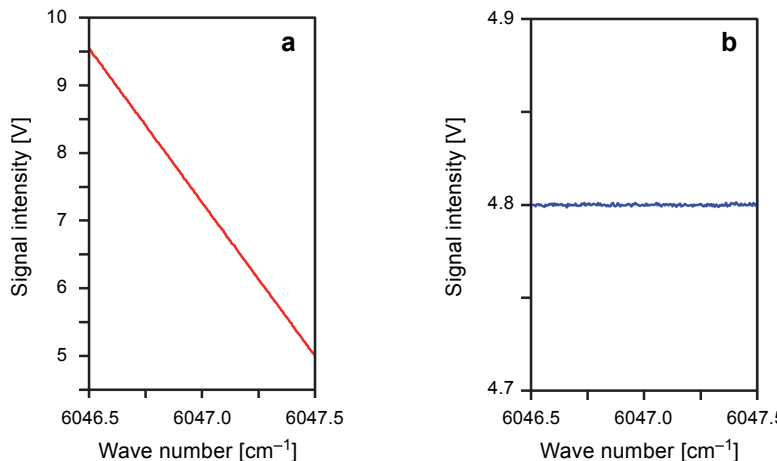


Fig. 5. The background signals for delayed differential detection (a) and phase-sensitive detection (b).

signals with the background, some variations that are independent of absorption, for example, the average laser intensity, detector sensitivity, signal amplification and laser transmission, can be excluded from the final result. The background signals belonging to delayed differential detection and traditional first harmonic detection are both shown in Fig. 5 for comparison. The dominant slope in Fig. 5a is caused by the saw-tooth current for wavelength sweep, while the DC bias shown in Fig. 5b is resulted from the sinusoidal signal for wavelength modulation.

The peculiarity of delayed differential detection is embodied by the contrastive results presented in Fig. 6 with the 1st derivative spectrum generated by the homemade electronic device (Fig. 6a) and the 1st harmonic detected by the lock-in amplifier (Fig. 6b). In Fig. 6b, the distortion of the 1st Fourier coefficient of absorption spectroscopy is characterized by the subtle asymmetry of wings and the conspicuous DC bias. The distortion is brought by the unwanted modulation of lasing intensity, which attends on the modulation of lasing wavelength. Compared with the asymmetry which only complicates the quantitative analysis of specimen, the absorption-independent RAM is more harmful for it may saturate the output of photodiode and thus limit the further amplification of weak absorption signals. Instead, the result of delayed differential detection in Fig. 6a exhibits the perfect symmetry and the nulled DC bias. The amplification of weak absorption for delayed differential detection, as a result, is not restricted by the background signal.

The intuitionistic definition of detection limit of a gas sensor is the gas concentration that can be detected while the SNR drops to 1. But, it is difficult to obtain the exact value through finite experiments. Instead of the practically measured detection limit, the theoretical value is easily deduced from the experiment using high-concentration specimen. For this, experiment using 500 ppm methane sample is performed, and the

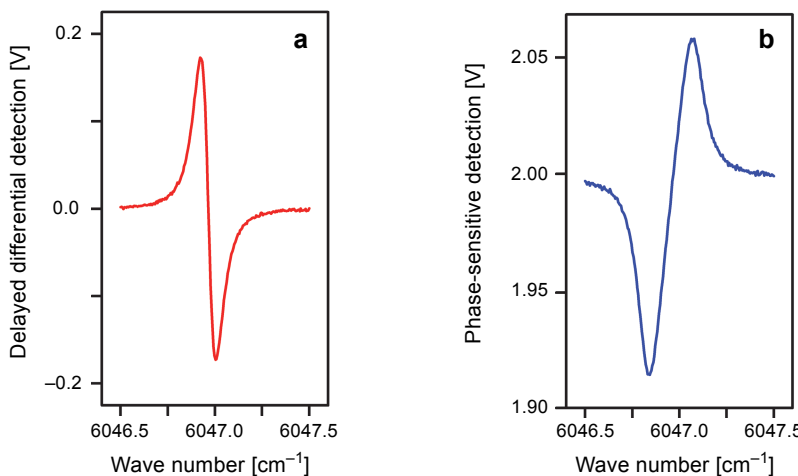


Fig. 6. Experimental results obtained from delayed differential detection (a) and phase-sensitive detection (b), using 1% CH<sub>4</sub> diluted by N<sub>2</sub>.

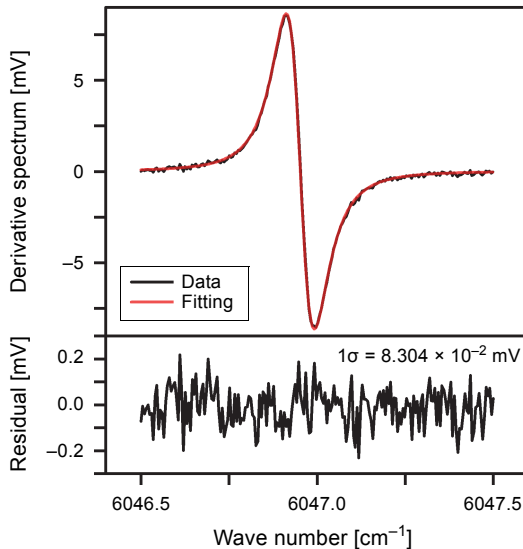


Fig. 7. Measured data and its fitting of the detector signal for  $\text{CH}_4$  with a concentration of 500 ppm. The fitting residual yields an equivalent SNR of 103.

result is shown in Fig. 7. The lower panel presents the residual of nonlinear fitting. Through carefully inspecting, the discrete data agree well with the fitting model. The peak is determined to be 8.553 mV, and the residual ( $1\sigma$ ) is calculated to be 83  $\mu\text{V}$ . Accordingly, it can be deduced that the SNR is 103. This indicates that the noise-limited minimal detectivity is about 4.9 ppm.

Figure 8 shows the dependence of detector signal on 7 methane samples in the concentration range from 500 ppm to 5%. The measured peak value of detector signal

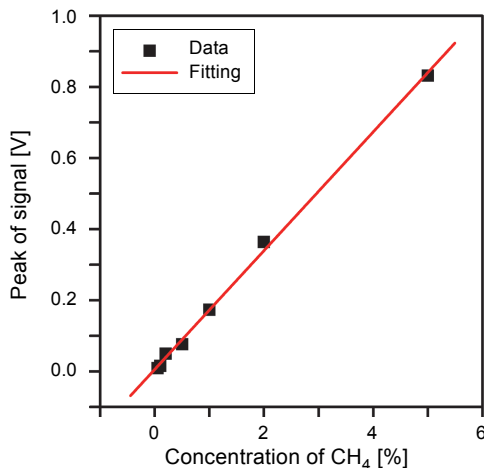


Fig. 8. Data and its fitting for describing the dependence of detector signal on  $\text{CH}_4$  mole fraction using 7 samples (0.05%, 0.1%, 0.2%, 0.5%, 1%, 2% and 5%).

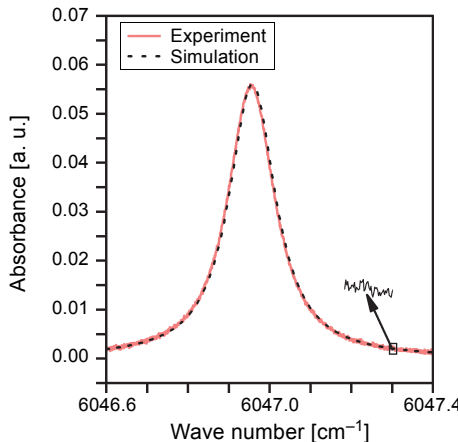


Fig. 9. Comparison of the experimental and simulated absorbance of 1%  $\text{CH}_4$  diluted by  $\text{N}_2$ , at pressure 1 atm and temperature 296 K.

shows very good linearity with methane concentration. A regression coefficient of  $R = 0.9977$  is derived from the linear fit that is described by

$$y = 0.1669x + 0.0061 \quad (13)$$

The curve of spectral absorbance derived from the first-order derivative spectrum integration is shown in Fig. 9, along with the simulation based on Voigt line shape. Spectral parameters involved in this simulation, including the center location of absorption line, absorption intensity, and broadening coefficient, are provided by the HITRAN04 database. It can be observed from Fig. 9 that, in the aspects of peak height and curve profile, the recovered absorption line profile shows excellent agreement with the simulation. Under a careful inspection, weak burrs are found in the measured line profile. This is mainly caused by the inherent noise of laser source.

## 5. Conclusions

This letter has demonstrated that, not only in principle but also in practice, TDLAS could be perfectly combined with the time-delayed differential detection for recovering the line shape function of absorption spectroscopy. An equivalent of the first-order derivative spectrum, from the integration of which the line shape function of absorption spectrum forms, is generated by a homemade circuit. Compared with WMS, here the modulating of laser driving current is replaced by setting the time delay constant of an all-pass filter, for the common purpose of first-order derivative spectrum generation but through a more convenient way. Moreover, the high-end lock-in amplifier used in WMS for the 1st harmonic detection is no longer needed, and the substitute is a simply designed circuit, which consists of an all-pass filter and an instrumentation amplifier. Attributed to the unique design of system architecture, in which the same gas cell and

photodetector is shared by the active and referenced paths, most of the common disturbers are cancelled by differential detection. In conclusion, the novel technique for absorption spectroscopy background-free, cost effectiveness and is characterized by low complexity.

*Acknowledgements* – This work was supported by the Scientific Research Project of Inner Mongolia University for the Nationalities (No. NMDYB17163). We would like to thank Editage ([www.editage.cn](http://www.editage.cn)) for English language editing.

## References

- [1] KOZLOWSKA K., LUKOWIAK A., SZCZUREK A., DUDEK K., MARUSZEWSKI K., *Sol-gel coatings for electrical gas sensors*, Optica Applicata **35**(4), 2005, pp. 783–790.
- [2] YADAV B.C., YADAV R.C., DUBEY G.C., *Optical humidity sensing behaviour of sol-gel processed nanostructured ZnO films*, Optica Applicata **39**(3), 2009, pp. 617–627.
- [3] LUCCHESENI A., GOZZINI S., *Methane diode laser overtone spectroscopy at 840 nm*, Journal of Quantitative Spectroscopy and Radiative Transfer **103**(1), 2007, pp. 209–216, DOI: [10.1016/j.jqsrt.2006.02.056](https://doi.org/10.1016/j.jqsrt.2006.02.056).
- [4] WRIGHT S., DUXBURY G., LANGFORD N., *A compact quantum-cascade laser based spectrometer for monitoring the concentrations of methane and nitrous oxide in the troposphere*, Applied Physics B **85**(2–3), 2006, pp. 243–249, DOI: [10.1007/s00340-006-2384-x](https://doi.org/10.1007/s00340-006-2384-x).
- [5] MASSIE C., STEWART G., MCGREGOR G., GILCHRIST J.R., *Design of a portable optical sensor for methane gas detection*, Sensors and Actuators B: Chemical **113**(2), 2006, pp. 830–836, DOI: [10.1016/j.snb.2005.03.105](https://doi.org/10.1016/j.snb.2005.03.105).
- [6] QIXIN HE, CHUANTAO ZHENG, HUIFANG LIU, BIN LI, YIDING WANG, TITTEL F.K., *A near-infrared acetylene detection system based on a 1.534 μm tunable diode laser and a miniature gas chamber*, Infrared Physics and Technology **75**, 2016, pp. 93–99, DOI: [10.1016/j.infrared.2016.01.006](https://doi.org/10.1016/j.infrared.2016.01.006).
- [7] PUSTELNY T., MACIAK E., OPILSKI Z., BEDNORZ M., *Optical interferometric structures for application in gas sensors*, Optica Applicata **37**(1–2), 2007, pp. 187–194.
- [8] WERLE P., SLEMR F., MAURER K., KORMANN R., MÜCKE R., JÄNKER B., *Near- and mid-infrared laser-optical sensors for gas analysis*, Optics and Lasers in Engineering **37**(2–3), 2002, pp. 101–114, DOI: [10.1016/S0143-8166\(01\)00092-6](https://doi.org/10.1016/S0143-8166(01)00092-6).
- [9] KRASNOSHCHEKOV S.V., VOGT N., STEPANOV N.F., *Ab initio anharmonic analysis of vibrational spectra of uracil using the numerical-analytic implementation of operator Van Vleck perturbation theory*, Journal of Physical Chemistry A **119**(25), 2015, pp. 6723–6737, DOI: [10.1021/acs.jpca.5b03241](https://doi.org/10.1021/acs.jpca.5b03241).
- [10] ASAOKAWA T., KANNO N., TONOKURA K., *Diode laser detection of greenhouse gases in the near-infrared region by wavelength modulation spectroscopy: pressure dependence of the detection sensitivity*, Sensors **10**(5), 2010, pp. 4686–4699, DOI: [10.3390/s100504686](https://doi.org/10.3390/s100504686).
- [11] CHUNGUANG LI, CHUANTAO ZHENG, LEI DONG, WEILIN YE, TITTEL F.K., YIDING WANG, *Ppb-level mid-infrared ethane detection based on three measurement schemes using a 3.34-μm continuous-wave interband cascade laser*, Applied Physics B **122**(7), 2016, article ID 185, DOI: [10.1007/s00340-016-6460-6](https://doi.org/10.1007/s00340-016-6460-6).
- [12] IDEHARA T., KHUTORYAN E.M., TATEMATSU Y., YAMAGUCHI Y., KULESHOV A.N., DUMBRAJS O., MATSUKI Y., FUJIWARA T., *High-speed frequency modulation of a 460-GHz gyrotron for enhancement of 700-MHz DNP-NMR spectroscopy*, Journal of Infrared, Millimeter, and Terahertz Waves **36**(9), 2015, pp. 819–829, DOI: [10.1007/s10762-015-0176-2](https://doi.org/10.1007/s10762-015-0176-2).
- [13] SHARMA R., MITRA C., TILAK V., *Diode laser-based trace detection of hydrogen-sulfide at 2646.3 nm and hydrocarbon spectral interference effects*, Optical Engineering **55**(3), 2016, article ID 037106, DOI: [10.1117/1.OE.55.3.037106](https://doi.org/10.1117/1.OE.55.3.037106).

- [14] SCHILT S., TOMBEZ L., TARDY C., BISMUTO A., BLASER S., MAULINI R., TERAZZI R., ROCHAT M., SÜDMEYER T., *An experimental study of noise in mid-infrared quantum cascade lasers of different designs*, Applied Physics B **119**(1), 2015, pp. 189–201, DOI: 10.1007/s00340-015-6021-4.
- [15] WILSON G.V.H., *Modulation broadening of NMR and ESR line shapes*, Journal of Applied Physics **34**(11), 1963, pp. 3276–3285, DOI: 10.1063/1.1729177.
- [16] ZE-WEI ZUO, YI HAO, SANG-JIN CHOI, MINHO SONG, YOUNG-CHON KIM, JAE-KYUNG, *Intensity modulation-based fibre optic vibration sensor using an aperture within a proof mass*, IET Science, Measurement and Technology **11**(1), 2017, pp. 49–56, DOI: 10.1049/iet-smt.2016.0167.
- [17] BEHERA A., ANBO WANG, *Calibration-free wavelength modulation spectroscopy: symmetry approach and residual amplitude modulation normalization*, Applied Optics **55**(16), 2016, pp. 4446–4455, DOI: 10.1364/AO.55.004446.
- [18] FAROOQ A., JEFFRIES J.B., HANSON R.K., *Measurements of CO<sub>2</sub> concentration and temperature at high pressures using If-normalized wavelength modulation spectroscopy with second harmonic detection near 2.7 μm*, Applied Optics **48**(35), 2009, pp. 6740–6753, DOI: 10.1364/AO.48.006740.
- [19] CHAKRABORTY A.L., RUXTON K., JOHNSTONE W., *Suppression of intensity modulation contributions to signals in second harmonic wavelength modulation spectroscopy*, Optics Letters **35**(14), 2010, pp. 2400–2402, DOI: 10.1364/OL.35.002400.
- [20] ROTHRMAN L.S., BARBE A., BENNER D.C., BROWN L.R., CAMY-PETYRET C., CARLEER M.R., CHANCE K., CLERBAUX C., DANA V., DEVI V.M., FAYT A., FLAUD J.M., GAMACHE R.R., GOLDMAN A., JACQUEMART D., JUCKS K.W., LAFFERTY W.J., MANDIN J.Y., MASSIE S.T., NEMTCHEV V., NEWNHAM D.A., PERRIN A., RINSLAND C.P., SCHROEDER J., SMITH K.M., SMITH M.A., TANG K., TOTH R.A., AUWERA J.V., VARANASI P., YOSHINO K., *The HITRAN molecular spectroscopic database: Edition of 2000 including updates through 2001*, Journal of Quantitative Spectroscopy and Radiative Transfer **82**(1–4), 2003, pp. 5–44, DOI: 10.1016/S0022-4073(03)00146-8.
- [21] BAIN J.R.P., JOHNSTONE W., RUXTON K., STEWART G., LENGDEN M., DUFFIN K., *Recovery of absolute gas absorption line shapes using tunable diode laser spectroscopy with wavelength modulation—Part 2: experimental investigation*, Journal of Lightwave Technology **29**(7), 2011, pp. 987–996.

Received February 20, 2018  
in revised form June 8, 2018